



International Symposium of Transport Simulation (ISTS'18) and the International Workshop on Traffic Data Collection and its Standardization (IWTDCS'18)

Analysis of sag bottleneck phenomena based on multiclass traffic state estimation

Moto Takashima^a, Yasuhiro Shiomi^{b,*}

^aGraduation School of Science and Engineering, Ritsumeikan University, 1-1-1 Nojihigashi, Kusatsu 525-8577, Japan

^bRitsumeikan University, 1-1-1 Nojihigashi, Kusatsu and 525-8577, Japan

Abstract

This study proposes a novel technique for analyzing traffic dynamics based on multiclass traffic state estimation. One of the most common causes of bottlenecks on Japan's roads are sags. Considerable scientific attention has been paid to the bottleneck phenomena at sags in terms of both their microscopic and macroscopic aspects. However, the mechanisms of traffic breakdown at sags are not understood in detail yet. This paper presents a data assimilation system using a particle filter in which online observations from fixed detectors and probe vehicles are combined with multiclass traffic flow simulations to analyze the traffic dynamics that contribute to congestion at sags. The application of a particle filter enables the monitoring of the hidden traffic state described by the unobservable parameters of traffic flow models. On the application of this method to an existing sag bottleneck section, we found that i) the estimation results are a good fit to observation data from both fixed detectors and probes, ii) the integrated use of multiple data source enables estimation accuracy to be improved, iii) the traffic capacity of the upgrade section is lower than that of the other sections and this tendency is more marked for heavy vehicles than for regular vehicles.

© 2018 The Authors. Published by Elsevier Ltd.

This is an open access article under the CC BY-NC-ND license (<https://creativecommons.org/licenses/by-nc-nd/4.0/>)

“Peer-review under responsibility of the scientific committee of the International Symposium of Transport Simulation (ISTS'18) and the International Workshop on Traffic Data Collection and its Standardization (IWTDCS'18)”

Keywords: Data assimilation; particle filter; multiclass traffic flow; probe data; sag

1. Introduction

Sags are geometric features in freeways where the gradient changes from downgrade to upgrade (Goñi-Ros et al., 2015). Since the sequence of gradient changes causes disturbances in the speed of traffic flow, the traffic capacity is

* Corresponding author. Tel.: +81-77-561-5094; fax:+81-77-561-2667.

E-mail address: shiomi@fc.ritsumei.ac.jp

lower at sags than in flat sections. Statistics show that more than 60% of traffic congestion on freeway networks in Japan is caused by sags. Over the last three decades, considerable scientific attention has been paid to both the microscopic (e.g., Ozaki (1993), Xing and Koshi (1995), Yoshizawa et al. (2011), and Goñi-Ros et al. (2014)) and macroscopic aspects (e.g., Koshi et al. (1981), Patire and Cassidy (2011), and Jin (2018)) of bottleneck phenomena at sags. A mechanism by which bottlenecks could form at sags would be: i) a vehicle unintentionally slightly reduces its speed in the upgrade section due to insufficient acceleration, ii) the vehicles behind decelerate accordingly, generating a shockwave, and iii) the shockwave propagates upstream, and traffic breakdown occurs. However, it remains challenging to identify with high accuracy exactly when and where a traffic breakdown will occur in a sag section. Because sag bottleneck phenomena are caused by a slight gradient change, the impact of the sag on speed may vary between vehicle classes depending on weight and power: one might reasonably expect that heavy vehicles will decrease their speed in upgrade sections more than regular vehicles. Thus, it is essential to monitor the traffic state class by class to recognize signs of a breakdown and take appropriate countermeasures dynamically to prevent or alleviate traffic congestion.

In this paper, we develop a data assimilation system that combines online observations and traffic flow simulations implementing the multiclass traffic flow model proposed by van Lint et al. (2008). This enables the traffic dynamics leading to congestion at sags to be understood better through estimation of the hidden parameters in traffic flow models. Both Eulerian observation data collected by fixed-point traffic detectors and Lagrangian observation data collected from a portion of commercial heavy vehicles along the target section are incorporated into the system. The data are dynamically assimilated to a macroscopic first-order multiclass traffic flow model, in which fundamental diagrams (FD) are independently defined for each cell and each class. The FD parameters are calibrated to fit the observations in a step-by-step process.

The rest of this paper is organized as follows. Section 2 outlines the data assimilation system. Section 3 details the data used by the assimilation system, and section 4 presents the results of the numerical analysis. The key findings are summarized in the final section.

2. OUTLINE OF DATA ASSIMILATION SYSTEM

The data assimilation system is composed of a system equation and an observation equation, as shown in Eq. (1).

$$\begin{cases} \mathbf{x}_t = f_t(\mathbf{x}_{t-1}) + \boldsymbol{\xi}_{t-1} \\ \mathbf{y}_t = h_t(\mathbf{x}_t) + \boldsymbol{\psi}_t \end{cases}, \quad (1)$$

where \mathbf{x}_t and \mathbf{y}_t are the values of the traffic state including the hidden parameters at time t and the observed values at time t , respectively, f_t and h_t are known functions, and $\boldsymbol{\xi}_t$ and $\boldsymbol{\psi}_t$ are mutually independent sequences with a normal distribution. Fig. 1 illustrates the data assimilation system schematically. For more details on the state of the art of data assimilation in the context of traffic flow simulation, see Seo et al. (2017).

2.1. System model

A first-order multiclass macroscopic traffic flow model, FASTLANE, proposed by van Lint et al. (2008) is applied as a system model and is combined with the observation system by way of a particle filter. It is assumed that each class has a specific FD. The traffic state of each cell is defined by the total equivalent density, which is the sum of the density of all standard-class car classes. Then, the total throughput is then calculated by passenger car unit, and they are assigned to each class on the basis of the incremental-transfer (IT) principle (Daganzo et al., 1997). A unique feature of FASTLANE is its definition of the passenger car equivalent. The equivalent coefficient of class i in cell j at time t , $\eta_j^i(t)$, is dynamically defined by Eq. (2) depending on the traffic state.

$$\eta_j^i(t) = \frac{s^i + t^i \cdot V_j^i(t)}{s^0 + t^0 \cdot V_j^0(t)}, \quad (2)$$

where s^0 , s^i , t^0 , and t^i are the length and the minimum time headway of a standard vehicle and vehicle class i , respectively.

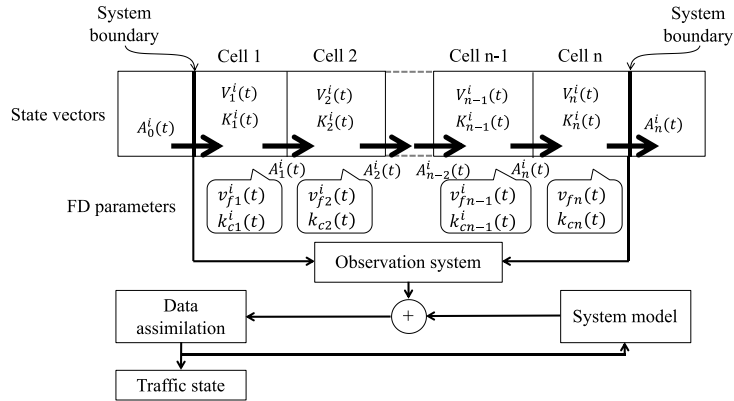


Fig.1. Schematic representation of the data assimilation system. $A_j^i(t)$, $V_j^i(t)$, and $K_j^i(t)$ represents traffic flow of class i from cell j to $j+1$ at time t , average speed of class i cell j at time t , and density of class i in cell j at time t , respectively. $v_{fj}^i(t)$ and $k_{cj}^i(t)$ are FD parameters, the free-flow speed and critical density of class i in cell j and time t , respectively.

2.2. Observation system

This study assumes the following realistic data-collection system. The observation data is collected by fixed detectors and probe vehicles. Fixed detectors can collect information on traffic volume and the speed of regular and heavy vehicles at specific locations at a fixed interval. The probe vehicle data is collected from commercial heavy vehicles in which GPS equipment is installed. Although the penetration rate of this technology is not very high and the data is limited to heavy vehicles, it is capable of providing speed data for cells in which traffic detectors are not installed.

2.3. Data assimilation system

The data assimilation is performed by way of a particle filter for several reasons: i) non-Gaussian distributions can be assumed for the unknown system parameters and noise, ii) the model can be nonlinear and it has been shown that the accuracy of traffic state estimation with this method is higher than with the extended Kalman filter (Takashima and Shiomi, 2017), and iii) given a sufficient number of particles, it can approximate to Bayesian optimization. In the proposed system, the parameters of the FD, which are separately defined for each cell, are considered to reflect the hidden state and are assumed to fluctuate independently over time. The calculation is performed as follows (for more detail, see Takashima and Shiomi (2017)):

- Step 1. Set the initial particles in a Gaussian distribution. One particle includes the FD parameters of each cell and each vehicle class.
- Step 2. Simulate one step to obtain the predicted values for the traffic state on the basis of the parameters given to each particle.
- Step 3. Following observation, extract the predicted values corresponding to the observations and calculate the likelihood value for each particle. Herein, we assume the observation values follow a multivariate normal distribution with a given variance-covariance matrix.
- Step 4. Assign a weight to each particle depending on likelihood, as shown in Eq. (3).

$$w_i = \frac{\exp[\ln \lambda_i - \ln \lambda_{\max}]}{\sum_j \exp[\ln \lambda_j - \ln \lambda_{\max}]}, \quad (3)$$

where w_i is the weight of the i th particle, λ_i is the likelihood of the i th particle, and $\lambda_{\max} = \max_i \lambda_i$.

Step 5. Output the weighted average of the particles as the estimated values.

Step 6. Resample the particles of the next step according to the weightings.

Step 7. Assign system noise to each particle, increment by one time step, and go back to step 3.

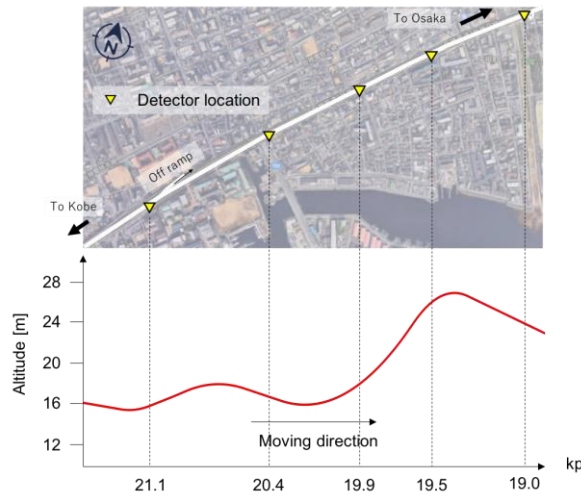


Fig. 2. Detector configuration and gradient in the target section

3. DATA DESCRIPTION

Observations were made in an eastbound, two-lane stretch of the Hanshin Expressway Route 3 on which single-head ultrasonic detectors collect height, time headway, and time occupancy data for individual vehicles. Vehicles are classified into two classes: regular vehicles, with a height of less than 2.3 m, and heavy vehicles, with a height of 2.3 m or more. Individual vehicle speed is roughly estimated assuming a class-specific vehicle length. Fig. 2 shows the detector configuration and geometry of the target section, in which a sag structure frequently causes traffic congestion starting from around the bottom of the sag at 20.1kp. Data were collected from June 6th to June 30th, 2016. Further analysis was conducted on data collected on June 30th because: i) the weather was fine, ii) a PML[†] was not operated, and iii) there was traffic congestion but no traffic accidents at the sag.

The relationship between the time occupancy per lane and the average class-specific speed can be calculated on the basis of individual vehicle data. Herein, the vehicle class is identified on the basis of the response time of an overhead ultrasonic sensor, and the lengths of regular and heavy vehicles are assumed to be 4.97 m and 8.2 m, respectively. Fig. 3 shows the variation in speed at the observation sites. A significant drop in speed to less than 50 km/h from 3 pm to 4 pm can be seen at 19.9 kp and upstream but cannot be seen at 19.5 kp and 19.0 kp. This indicates that the bottleneck was located in the section between 19.9 kp and 19.5 kp. Fig. 4 shows the class-specific fundamental relationship between time occupancy and average speed. When time occupancy is less than 30% and so traffic is almost free-flowing, a significant difference in speed between regular and heavy vehicles is seen; however, as time occupancy increases, this gap gradually reduces until their speeds are almost the same in traffic congestion. It is also interesting to note that the speed of heavy vehicles is not sensitive to time occupancy in the free-flow region.

Probe data, including latitude, longitude and speed per second were collected from a subset of commercial heavy vehicles. Heavy vehicles make up, on average, 11.2% of all vehicles, and the penetration rate of GPS equipment in the heavy vehicle class is 5.7% on average. It must be noted that the speed values collected from probe vehicles are significantly higher than the speeds derived from the detector data. This may indicate that the average length assumed for heavy vehicles, 8.7 m, is unrealistic. Therefore, we adjusted the probe speed values to match the speeds derived from the detector data. The black dots in Fig. 3 show the modified speed of individual probe vehicles. It can

[†] A pace-maker light, which is a sequence of blinking LED lights that seems to be moving at a fixed speed. PMLs are installed for the purpose of mitigating traffic congestion by encouraging drivers to maintain a constant driving speed at sag sections (Kameoka et al. (2015)).

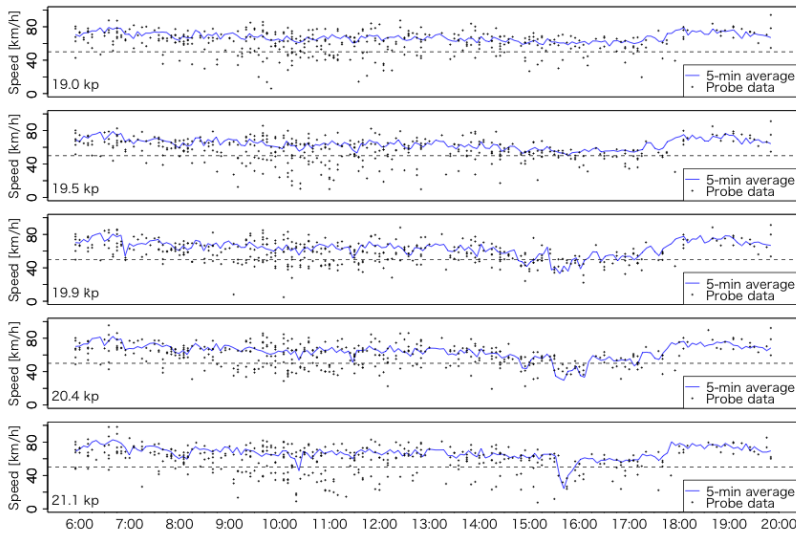


Fig. 3 Speed variation at the observation sites on June 30th, 2016.

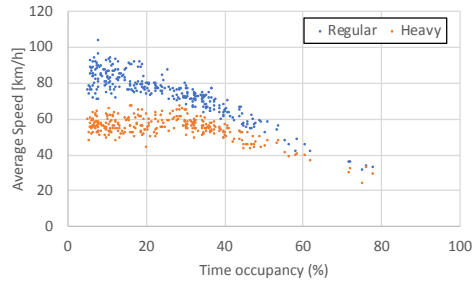


Fig. 4. Class-specific relationship between time occupancy and average speed at 20.4 kp on June 30th, 2016.

be seen that the probe-sourced speeds are in good accordance with the 5-min average speeds, especially in the congested traffic state.

4. NUMERICAL ANALYSIS

4.1. Settings of the data assimilation system

The section from 20.4 kp to 19.0 kp is targeted for numerical analysis so as to include the sag bottleneck and exclude the effect of an off-ramp at 20.9 kp. The target time duration is set to 3,600 sec before and after traffic breakdown because the objective of the numerical analysis is to understand sag bottleneck phenomenon. As Fig. 5 shows, to facilitate this, the target section is divided into five 280 m-long cells. Note that the detectors do not exactly correspond to the cells; however, this can be considered as a component of the observation error. The time step and the maximum speed are set to 10 sec and 100 km/h, respectively. It is assumed that the FD follows Drake's model as shown in Eq. (4).

$$v^i = v_f^i \cdot \exp \left[-\frac{1}{2} \cdot \left(\frac{k^i}{k_c^i} \right)^2 \right], \quad (4)$$

where v_f^i and k_c^i are the FD parameters of free-flow speed and critical density for vehicle class i , respectively. The initial values used for the free-flow speeds are 80 km/h for regular cars and 60 km/h for heavy vehicles. The initial value for the critical density is 75 veh/km in passenger equivalent units. The settings for vehicle length in Eq. (2) are as follows: s^0 and t^0 are 4.97 m and 1.0 sec for regular vehicles and s^1 and t^1 are 8.2 m and 1.4 sec for heavy vehicles, respectively.

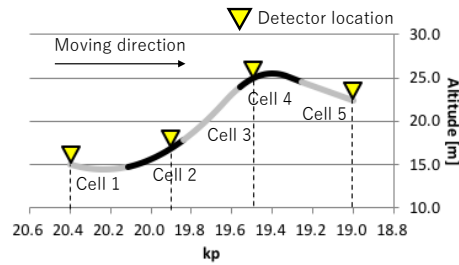


Fig. 5. Cell and detector configuration in the target section

Table 1. PF parameter settings.

Standard deviations of system noise			Standard deviations of observation noise		
Critical density	0.4	[veh/km]	Throughput of regular vehicles	3.0	[veh/10 sec]
Free-flow speed of regular vehicles	1.38	[km/h]	Throughput of heavy vehicles	1.5	[veh/10 sec]
Free-flow speed of heavy vehicles	1.38	[km/h]	Speed of regular vehicles by detectors	7.0	[km/h]
			Speed of heavy vehicles from detectors	6.0	[km/h]
			Speed of heavy vehicles from probe data	6.0	[km/h]
Number of particles	5,000				

Table 1 summarizes the settings of the particle filter. The standard deviations of the noise parameters are determined to obtain accurate estimation results. Except for cell 3, each cell has a corresponding traffic detector by which the throughputs and average speeds over 10 sec are collected and used for the data assimilation. If probe records are available at the location of cell 3 for a 10 sec window, the average of the probe speed data is used as that cell's observation value. Thus, the gap in detector coverage is compensated for by fusing the different data sources.

4.2. Estimation results

The estimation results are validated by comparing the throughput and speeds from the detector at 19.9 kp and the speed collected from probe data in cell 3 with the results of the traffic state estimation (Fig. 6). The estimation results for regular and heavy vehicles both closely correlate with the observation data once the observation noise has been eliminated. It is particularly noteworthy that the estimation of the speed in cell 3 matches the observed data with high accuracy in spite of the sparseness of the observation data. Without probe data for cell 3, the estimation results would tend to be unstable because throughput in cells 2 and 4 would be the only constraint on the traffic state of cell 3. Thus, the accurate estimation results in Fig. 6(d) highlight the importance of integrated usage of multiple data sources.

Fig. 7 depicts the estimated speed contours for regular vehicles, large vehicles and the difference between them. This figure shows that traffic breakdown occurred at time step 222, and the front of the congestion queue remained at cell 2 subsequently, though there was some minor fluctuation in its position. Additionally, a considerable speed reduction can be seen around time steps 18–52; however, this traffic state propagates downstream and the difference in speeds by class is not large, implying that this speed reduction may be attributable to the presence of a few slow vehicles. On the other hand, in the time steps around 171–222 just before the traffic breakdown, the difference in speed between regular vehicles and heavy vehicles becomes extremely high at cell 3. This implies that disturbance of the traffic flow and subsequent traffic breakdown were caused by a reduction in the speed of heavy vehicles in the upgrade section in cell 3.

To examine this in more depth, Fig. 8 illustrates variations in the estimated traffic capacity for each type of vehicle, q_c , as calculated with Eq. (5),

$$q_c = k_c \cdot v_f \cdot e^{-\frac{1}{2}} \quad (5)$$

This is based on Eq. (4); k_c and v_f are obtained dynamically as the results of the particle filter. Note that each cell has its own FD parameters, and it is assumed in the estimation process that they vary independently. This figure indicates that traffic capacity in cell 3 tends to be the lowest before traffic breakdown, and this tendency is

particularly pronounced for heavy vehicles. We infer that the steep upgrade section causes heavy vehicles to reduce their speed, which may trigger traffic breakdown at the sag. It is also interesting to note that the traffic capacity for regular vehicles slightly decreases just after the traffic breakdown, whereas the traffic capacity for heavy vehicles remains stable. This suggests that regular vehicles experience a greater capacity drop than heavy vehicles do, although further investigation may be necessary to verify this.

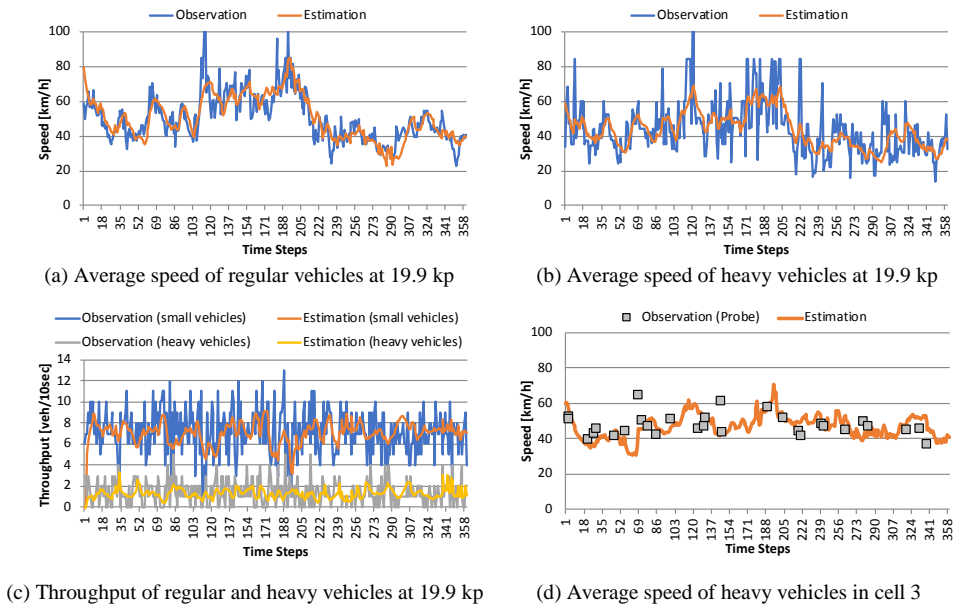


Fig. 6. Results of traffic state estimation.

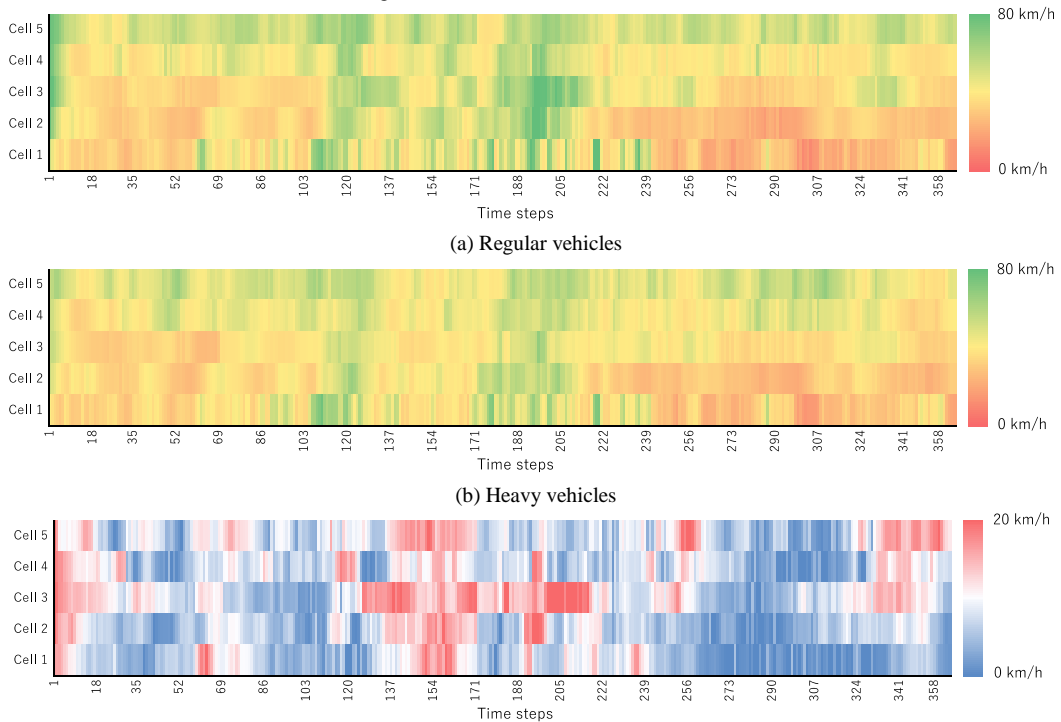


Fig. 7. Estimated speeds.

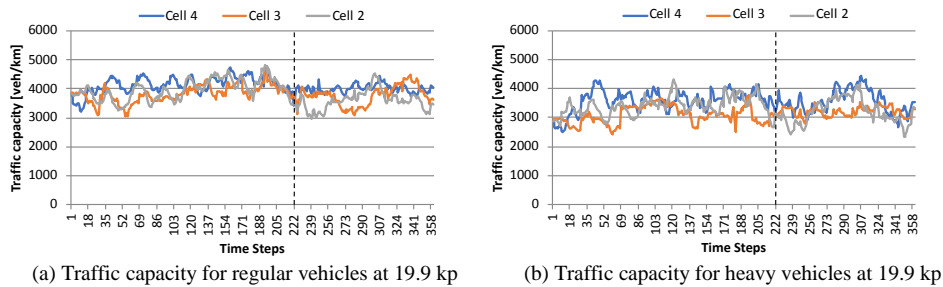


Fig. 8. Time-series variation in traffic capacity.

5. CONCLUSION

This paper proposes a novel method of analyzing sag bottleneck phenomena in which online observation data from fixed detectors and probe vehicles are combined with multiclass traffic flow simulation by way of a particle filter. As a result of the application of this method to an existing sag bottleneck section, we conclude that i) the estimation results are a good fit to observation data from both fixed detectors and probes, ii) the integrated use of multiple data sources enables more accurate estimation, iii) the traffic capacity of the upgrade section is lower than that of the other sections, and this tendency is more marked for heavy vehicles than regular vehicles. In addition, the results indicate that disturbance in traffic flow and resulting traffic breakdown at a sag may arise due to the significant difference in speed between regular and heavy vehicles. In future work, we will apply the method to further examples to further validate the results of this investigation.

Acknowledgements

This work was supported by JSPS KAKENHI Grant Number JP15H04061 and JP16H04433. The authors appreciate Hanshin Expressway Co. Ltd. and Fujitsu traffic & road data service Ltd. for the data provision.

References

- Ros, G.B., Knoop, V., Shiomi, Y., Takahashi, B., van Arem, B., Hoogendoorn, S.P., 2014. Modeling traffic at sags. *International Journal of ITS Research*, pp.1-11.
- Daganzo, C.F., Lin, W., Del Castillo, J., 1997. A simple physical principle for the simulation of freeways with special lanes and priority vehicles. *Transportation Research Part B* 31 (2), 105–125.
- Jin, W.-L., 2018. Kinematic wave models of sag and tunnel bottlenecks. *Transportation Research Part B: Methodological* 107, pp.41-56.
- Koshi, M., Iwasaki, M., Ohkura, I., 1983. Some findings and an overview on vehicular flow characteristics. In: Hurdle, V. F., Hauer, E., Steuart, G. N. (Eds.), *Proceedings of the Eighth International Symposium on Transportation and Traffic Theory*, University of Toronto Press, Toronto, 403-451.
- Kameoka, H., Oneyama, H., Sakurai, M., Tsuji, M., 2015. Effect of Dynamic Control of Light-Emitting Devices Installed along a Road Shoulder on Congestion Relief, *Journal of the Eastern Asia Society for Transportation Studies*, Vol. 11, pp. 1919-1930, 2015.
- Ozaki, H., 1993. Reaction and anticipation in the car-following behavior. *Proceedings of 12th ISTTT (Berkeley)*, 349-366.
- Patire, A. D. and Cassidy, M. J., 2011. Lane changing patterns of bane and benefit: Observations of an uphill expressway. *Transportation Research Part B: Methodological*, vol. 45, no. 4, pp. 656–666.
- Takashima, M., Shiomi, Y., 2017. Monitoring Traffic Flow Dynamics at Sags: Data Assimilation Approach. *Proceedings of ISTS & IWTDCS 2016*, Jeju, Korea.
- Seo, Toru, Bayen, Alexandre, Kusakabe, Takahiko, and Asakura, Yasuo, 2017. Traffic state estimation on highway: A comprehensive survey. *Annual Reviews in Control*. Vol.43, pp. 128-151.
- van Lint, H., Hoogendoorn, S.P., and Schreuder, M., 2008. Fastlane – A new multi-class first order traffic flow model, the proceedings of the 87th meeting of the Transportation Research Board, pp.13-17.
- Xing, J., Koshi, M., 1995. A study on the bottleneck phenomena and car-following behavior on sags of motorways. *Journal of Infrastructure Planning and Management* 506 (IV-26), 45-55 (in Japanese).
- Yoshizawa, R, Shiomi, Y, Uno, N, Iida, K and Yamaguchi, M., 2011. Analysis of car-following behavior on sag and curve sections at intercity expressways with driving simulator”, *Int. Journal of Intelligent Transportation Systems Research*, vol. 10, no. 2, pp. 56–65.